Maximal curvature and crystal orientation on directionally solidified dendrites

A. Pocheau, J. Deschamps, and M. Georgelin
IRPHE, Aix-Marseille Université and CNRS, 49 rue Joliot-Curie, BP 146, F-13384 Marseille, France
(Received 21 July 2009; revised manuscript received 9 February 2010; published 28 May 2010)

We experimentally address the locations of maximal curvature on crystalline cellular or dendritic interfaces that directionally grow in a thin sample of a transparent material. Local curvatures are determined on the whole dendrite tips by considering the intersection of nearby normals. It is found that, at the location of the curvature maximum, the interface normal points toward a particular direction solely set by the crystal lattice and equal in practice to the dendrite growth direction at large pulling velocity. This property is independent of the growth conditions (thermal gradient, velocity, dendrite spacing, and crystal orientation). It enables crystal orientations to be recovered from dendrite shapes and provides a bridge to understand the implications of anisotropy on the forms and orientations of directionally solidified dendrites.

DOI: 10.1103/PhysRevE.81.051608 PACS number(s): 68.70.+w, 47.20.Hw, 82.40.Ck

I. INTRODUCTION

Many materials displayed in nature or in industry result from the solidification of a dilute melt in a nonuniform temperature field. They then refer to directional solidification as opposed to the free solidification exhibited when the temperature field is uniform. Examples include cast objects produced in metallurgy [1] or rocks solidified in lava lakes or in the earth crust [2]. In each of them, the efficiency of melt freezing drives the velocity of isothermal lines with respect to the liquid phase and thus the actual velocity of the solidification interfaces. This provides interface shapes aligned on an isotherm at low solidification velocity but undergoing, above a critical velocity, the spontaneous formation of cells [3]. Beyond another velocity threshold [4], a secondary instability makes these cells emit sidebranches, according to which they are called dendrites.

Dendrites actually stand as the dominant microstructure of directional solidification in dilute alloys. In particular, they occur on any material involving rough interfaces and on most of their usual ranges of solidification velocities [1]. Interestingly, as the impurity concentrations vary on these curved interfaces, solidification results in the formation of composition modulations in the solid at the dendrite scale with noticeable implications on the physical and mechanical properties of the alloys. Accordingly, dendrites stand both for the spontaneous emergence of time-dependent forms at a microscale and for a source of material microsegregation. For these reasons, their nature appears both challenging on a fundamental ground and of paramount importance for metallurgical purposes.

Interestingly, crystal anisotropy, no matter large or small, no matter relative to surface tension or to kinetic undercooling, has proved to be essential to dendrites. In particular, it has been recognized as playing a major role in their very existence [5–10], instead of seaweed structures or doublons otherwise [11,12]. However, beyond this existential issue, it also proved to monitor the orientation and the overall shape of dendrites. For instance, in the free solidification of isothermal media, dendrites are found to grow along specific crystalline directions [1] with respect to which they are usually symmetric. They then display a close to parabola tip [13–15]. Sometimes however, they appear to grow along atypical directions for reasons still referring to anisotropy [16].

In directional solidification, however, a fundamental difference raises from the existence of two characteristic directions for monitoring growth: the direction of the thermal gradient **G** and a direction **a** set by the crystal orientation. Their competition is then parametrized by microstructure spacings and growth velocities. In particular, at large solidification velocities, all dendrites grow along the direction **a**, whatever the direction of **G** [1,17–23], and with a close to parabola tip [24]. In contrast, at low velocities, microstructures are found to grow close to the heat flow direction **G**, whatever the direction **a** [18–22], and with a digitlike tip [25–29]. In between, as the solidification velocity increases, they then rotate from the direction **G** to the direction **a** [17–22] while raising their inclination, their tip curvature, their asymmetry, the amplitude of their secondary branches and the distance to their neighbors [20–22].

Crystal anisotropy, although extremely weak in terms of temperature modulations of solidification interfaces, thus appears surprisingly efficient in governing the growth directions and the shapes of directionally solidifying cells and dendrites. The way it acts on microstructures however shows peculiar properties. In particular, the rotation of dendrites proved to satisfy an internal symmetry, a scale invariance with respect to a Péclet number, whose validity englobes the whole parameter ranges [20–22]. This first indicates that growth directions refer to a single physical regime, whatever the growth conditions or the cellular or dendritic nature of the microstructure, so that the issue might be simpler to understand that might have been feared. However, this rotation law also suggests that the magnitude of the thermal gradient and of the crystalline anisotropy play no role in the dendrite orientations, even if their respective directions **G** and **a** actually do [21]. If so, this strange ambivalence would indicate that thermal gradient and crystal anisotropy act as singular perturbations in the growth system, so that pointing out their respective role might well be a subtle analytical task.

On a general viewpoint, the intrinsic difficulty in dealing with the implications of crystalline anisotropy on directional dendrites traces back in the scale difference inherent to the involved phenomena: the molecular scale for crystal lattice, the micrometric scale at least for dendrites and the millimeter

scale or more for the thermal gradient. In particular, determining the interplay between thermal gradient and crystal orientation on dendrites turns out simultaneously handling the implications of a macroscopic phenomenon (the heat flow) and of a microscopic modulation (the crystal-induced anisotropy) on a mesoscopic object (the cell or the dendrite). In addition, the hardness of this issue is enhanced by the fact that a free boundary is sought for in a context where nonlocal interactions are provided between distant interface parts by the diffusive and advective solute transports.

A way to render this issue more tractable might be to reduce its extension in scale space by determining a mesoscopic implication of crystal orientation. Then, the coupled roles of heat flow direction and crystal lattice orientation on solidification could be handled at a single mesoscopical scale by using this crystal-induced property together with a constant thermal gradient. A natural candidate for that is the dendrite shape whose crystal-induced features could be used as additional conditions for solving the free-boundary problem. This has motivated us to seek whether crystal anisotropy could yield a definite geometrical implication on dendrites, preferentially a local implication for simplifying the further understanding of this nonlocal growth system. This led us to investigate the extremal features of dendritic interfaces and, especially, that of lowest differential degree: the localization of the maximal curvature.

The central issue of our study has thus consisted in determining how, in directional solidification, the location of the maximal interface curvature evolves with the growth conditions on dendrites and in comparing this evolution with that of the dendrite growth direction.

Would the study had taken place in free growth, its conclusions had been more direct. As the thermal gradient vanishes, the only specific orientations that remain are provided by the crystal lattice. Except in case of competition between cubic harmonics of the interfacial energy [16] or between kinetic and surface tension anisotropy [30], dendrites grow along a principal crystallographic axis **a** on which the interfacial stiffness is minimal. They then display a symmetrical form with respect to this axis and thus a maximal curvature there. The growth direction $\mathbf{V}_g$ of dendrites, their normal direction $\mathbf{n}_c$ at the location of their maximal curvature and the crystalline direction **a** are then all the same: $\mathbf{n}_c//\mathbf{V}_g//\mathbf{a}$.

In the present directional system, things are complexified by the presence of two directions **G** and **a** that compete in fixing the specific directions of a dendrite, i.e., its growth direction $\mathbf{V}_g$ and its normal direction $\mathbf{n}_c$ at its highest curvature location. Several possible outcomes may then be expected: (i) the maximal curvature may point toward **G**: $\mathbf{n}_c//\mathbf{G}$; (ii) it may follow the rotation of the growth direction $\mathbf{V}_g$ from **G** to **a**: $\mathbf{n}_c//\mathbf{V}_g$; (iii) it may remain pointing toward the crystal defined direction **a**: $\mathbf{n}_c//\mathbf{a}$; (iv) it may exhibit an intermediate behavior.

In the former case, $\mathbf{n}_c//\mathbf{G}$, the most curved point would be independent of crystal orientation even at large velocities. In the second case, $\mathbf{n}_c//\mathbf{V}_g$, the quickest growing point (whose normal points toward $\mathbf{V}_g$) would be, as in free growth, the most curved point. But it would no longer point toward a crystal defined axis. In the third case, $\mathbf{n}_c//\mathbf{a}$, the quickest growing point would no longer be confused with the most curved point, except at large velocity where $\mathbf{V}_g//\mathbf{a}$. Finally, in the last case, no simple behavior might be *a priori* expected.

Nevertheless, it is usually expected that, at large velocity, the dendrite tip stands as the most curved part of the interface with a normal pointing toward the crystal defined direction **a**. On the other hand, at low velocity, the growth direction $\mathbf{V}_g$ is known to match the thermal gradient direction **G** whatever the crystal orientation. This supports a cell form corresponding to the digitlike solution proposed in the low Péclet number regime [25] and with a maximal curvature pointing to direction **G** too. This would therefore select the case (ii), $\mathbf{n}_c//\mathbf{V}_g$, or the case (iv). We shall find that this is contradicted by our experiment.

In this paper, we have experimentally determined the local curvatures displayed along the tips of directional cells and dendrites from a geometrical method based on the intersection points of neighbor normals. We have surprisingly found that the *maximum* of the interface curvature is reached at a point whose interface normal **n** keeps *aligned* with the crystal defined direction **a**, *whatever* the solidification velocity, the dendrite spacings, their asymmetry, or the sidebranch development: $\mathbf{n}_c//\mathbf{a}$. This property, which enables the crystal orientation to be recovered from the dendrite shapes, proved to extend to transient states and to dendritic patterns exhibiting different spacings. It thus provides a definite geometrical implication of crystal anisotropy on microstructure shapes which is both independent of the growth conditions and robust to disturbances. It may therefore open a valuable track for understanding the role of anisotropy on microstructure features.

Section II reviews the main difference between free and directional solidification regarding the present issues and states the expectation that can be drawn as to the location of maximal interface curvature in directional solidification. The setup and procedures used in our experiment are then described in Sec. III and the evolutions of the forms and the growth directions of microstructures are reported in Sec. IV. Section V then discusses the geometrical method applied for measuring local curvatures. Applying it in Sec. VI provides a quantitative evidence that the interface normals at the location of the curvature maxima coincide with the crystal defined direction **a**. This is followed by a discussion and a conclusion about these results.

II. CURVATURE, GROWTH DIRECTION, AND ANISOTROPY

The implications of anisotropy on the growth direction of dendrites or on the location of their maximal curvature has mainly been addressed in free solidification and comparatively much less in directional solidification. Yet, this latter case involves a major difference that deserves a special attention: the presence of an additional prescribed direction, that of the thermal gradient **G**. To better grasp its specificity, we first review the main conclusions reported in free growth on this topic, then emphasize the implications brought about by a thermal gradient and finally conclude about the expectations that may be drawn in directional solidification on the

evolutions of the most curved interface point.

The main information regarding the shape and the location of the solidification interface comes from the Gibbs-Thomson relationship which relates its temperature T_I to its solutal concentration c_I up to capillary and kinetic corrections

$$T_I = T_M - mc_I - \frac{T_M}{Q}(\tau_1\kappa_1 + \tau_2\kappa_2) - \beta V_n. \quad (1)$$

Here, T_M denotes the melting temperature of the pure solvent, $-m$ the liquidus slope, Q the volumic latent heat, $i=1,2$ the indexes of the two principal planes, $\tau_i=\gamma+\partial^2\gamma/\partial\alpha_i^2$ the interface stiffnesses, γ the surface tension, α_i the polar angles in the principal planes, κ_i the interface curvatures, and V_n the normal interface velocity. The two last terms of the right hand side, respectively, stand for the capillary and kinetic corrections to the interface temperature. They involve a dependence of the stiffnesses τ_i and of the kinetic factor β on the relative orientation of the interface with respect to the crystal, i.e., on the angles $\theta_j=(\mathbf{a}_j,\mathbf{n})$ between the directions of the lattice principal axes $\mathbf{a}_j$, $j=1,2,3$, and the interface normal $\mathbf{n}$: $\tau_i\equiv\tau_i(\theta_j)$, $\beta\equiv\beta(\theta_j)$.

This orientational dependence must satisfy global rotation and reflexion symmetries as well as the discrete symmetries consistent with those of the crystal lattice. For a cubic crystal and at the lowest order in an expansion in the components (n_1,n_2,n_3) of the interface normal $\mathbf{n}$ in the lattice frame, it expresses as a function of the fourth-order harmonic combination $(n_1^4+n_2^4+n_3^4)$ or, equivalently, of the fourth-order harmonic function $f_4(\mathbf{n})=4(n_1^4+n_2^4+n_3^4)-3$ [31]. The variables $\chi\equiv\gamma$, τ_i, or β then write

$$\chi(\mathbf{n}) = \chi_0[1+\xi_0 f_4(\mathbf{n})] + o(\xi_0) \quad (2)$$

with (χ_0,ξ_0) labeled (γ_0,ϵ_4) for surface tension, $(\tau_0,-\epsilon_c)$ for stiffnesses, and $(\beta_0,-\epsilon_k)$ for the kinetic factor. When the principal planes are crystallographic planes (1,0,0), the angular dependence $f_4(\mathbf{n})$ then reduces at the dominant order to a sinusoidal modulation $f_4(\mathbf{n})=\cos(4\theta_j)$. However, in more general situations, higher order terms may need to be considered.

It should be noted that surface tension or kinetic corrections to the temperature interface are weak and that their anisotropic modulations are even weaker. In particular, for the present solvent, succinonitrile, the values of surface tension and of its anisotropy coefficient amount to $\gamma_0=\tau_0=8.94\times10^{-7}$ J.cm^{-2} [32] and $\epsilon_4=(0.55\pm0.15)\%$ [33]. For a typical radii of curvature ρ of dendrite tips, of order ten micrometers, the mean surface tension correction $\delta T=\gamma_0 T_M/Q\rho$ appears as low as 6 mK since $T_M=331.23$ K [34] and $Q=46.7$ J.cm^{-3} [35]. Surface tension anisotropy thus acts as a weak modulation ($\epsilon_c=15\epsilon_4=8\%$) of a tiny relative temperature correction ($\delta T/T_I\approx\gamma_0/Q\rho\approx2.10^{-5}$). In particular, in the thermal gradient of 70 K.cm^{-1} that has been used here, this correction is equivalent to a shift in dendrite tip position lower than a micrometer and its modulation to about 70 nanometers. Nevertheless, it surprisingly proves to have a considerable effect on the growth direction and, as we shall see, on the location of the most curved point. Kinetic effects have not been quantitatively reported for succinonitrile but they are known to be even smaller than the capillary effects. For this reason, we shall only focus attention on the latter below.

A. Free growth

We consider the free solutal growth of a melt in an isothermal medium. Without interfacial corrections to the interface temperature, dendrites steadily growing at velocity V then involve a parabolic shape whose curvature radius ρ at the tip satisfies the Ivantsov relationship [13]: $\rho V=2DP(\Delta_I)$ where Δ_I denotes the interface undercooling, D the solutal diffusion coefficient, and $P(.)$ an explicit function derived from the growth system. At a given undercooling, a family of solutions (ρ,V) may thus arise whereas a single solution is found experimentally [34]. This theoretical degeneracy comes from an absence of characteristic scales that breaks down once surface tension is considered. In particular, stability theories suggest the existence of a constant stability parameter σ such that $\rho^2\sigma=2l_D d_0$ where d_0 denotes the capillary length [5]. Combined with the Ivantsov scaling, this yields the following determination for the dendrite velocity: $d_0V=D\sigma P^2(\Delta_I)$. Some anisotropy is however required to obtain a stable solution [7]. Let us address its specific effects on both the growth direction and the location of the largest curvature of dendrites.

1. Symmetric dendrites

Simple conclusions may first be easily reached by considering dendrites that are symmetric with respect to their growth axis. Then, by symmetry, the interface point located on the growth axis involves an extremal solute concentration and an extremal curvature. From the Gibbs-Thomson relation (1), this also implies an extremal stiffness and thus an extremal capillary length d_0. However, following stability theories [5,7], d_0V is a constant at given undercooling, so that a maximal growing velocity must be reached for a minimal d_0, i.e., for a minimal stiffness. Selecting this solution for dynamical reasons yields dendrites growing along a principal crystalline axis and with their largest curvature located at their tip.

2. Microscopic solvability theory

Drawing on the linearity of the growth system with respect to solute concentration enables to recast it into a boundary integral equation by use of Green's functions. Interestingly, in the two limit cases of one-sided model (no diffusivity in the solid phase) and of the symmetric model (equal diffusivity in both phases), this equation reduces to a closed integrodifferential equation for the interface position. It then offers the opportunity of directly studying the effects of surface tension and anisotropy on the dendrite shape. Considering a sinusoidal angular dependence of surface tension and asking for a regular shape at the dendrite tip with no angulous point then called for the existence of anisotropy $(\epsilon_c\neq0,\epsilon_k\neq0)$ to obtain a solution [7,9,30]. This implied the selection of both the microsolvability parameter σ (and thus of the dendrite tip radius ρ) and of the dendrite growth di-

rection. In particular, for $\epsilon_k \geq 0$ and $\epsilon_c \neq 0$, the dendrite could only grow on the principal crystalline axes whereas for $\epsilon_k < 0$, it was found to grow on these axes at low velocity but on secondary crystalline axes at large velocity [30]. In any of these cases however, the dendrite was found to be symmetric with respect to its growth axis, with therefore a maximum curvature at its tip.

3. Competition between surface tension harmonics

It appears however that the sinusoidal angular dependence of the capillary length $d_0(\theta)$ used in the above microscopic solvability theory is only the dominant order of a more general systematic expansion. In particular, in a three-dimensional (3D) approach of dendrite growth, expansion of the interface stiffness in terms of spherical harmonics points out the possibility of a competition between the effects of the two first dominant terms when they actually support growth in different directions, i.e., one on a principal crystallographic axis and the other on a secondary axis [16]. It might be guessed that this competition could be solved by identifying the selected growth direction with the minimal stiffness direction. This, however, only provides the main tendencies, i.e., the growth on principal or secondary crystalline directions, but misses the intermediate atypical directions that are provided at the transition between these two directions in the parameter space [16]. In the former case, dendrites are symmetric with respect to their growth directions and thus display a maximal curvature at their tip; in the latter case of atypical directions, dendrites are no longer symmetric so that their tip no longer coincides with a maximal curvature.

4. Growth direction and maximal curvature

It thus appears that, already in free growth, the determination of growth direction and of maximal curvature stands as a subtle issue capable of providing several outcomes as soon as a competition between different tendencies is in order. In particular, there exists no general principle capable of yielding a simple definite answer as for instance the extremalization of stiffness or of tip undercooling. This warns about the difficulty in determining the analogous behaviors in directional growth where the competition between the respective orientations of the crystal lattice and of the heat flow sets the rule.

B. Directional growth

In directional growth, another specific direction, that of the thermal gradient $\mathbf{G}$, is added to the system. Judging from the effects of the competition between primary and secondary crystallographic axis in free growth, one may thus *a priori* expect large implications of the competition between crystal orientation and heat flow direction.

Apart from introducing a specific direction, the thermal gradient also yields the solidification interface to structure itself in a cellular or dendritic array, above the onset of planar interface instability. This provides a mesoscopic scale, the cellular or dendritic spacing Λ, which helps judging about the degree of nonlocality of the growth system. For this, the spacing Λ has to be compared to the natural length provided by the interplay between advection and diffusion, i.e., the diffusion length $l_D = D/V$, which basically corresponds to the influence length of a point source in the growth system. This comparison is performed in the Péclet number $\mathrm{Pe} = \Lambda V/D$.

1. Large Péclet number: $\mathrm{Pe} \gg 1$

At large Péclet number, the influence length of an interface point, l_D, is much smaller than the microstructure scale Λ. Apart from cumulative effects of diffusion fluxes, the interface dynamics may then be considered as local on the scale l_D. The effect of the thermal gradient on this scale may then be evaluated by comparing the resulting temperature difference across it, $\delta T = G l_D$, to the shift in equilibrium temperature (1) implied by solute concentration, mc_I, and by surface tension, $\tau\kappa T_M/Q$. It then appears that $\delta T \ll mc_I$ requires $V \gg V_c$ but that $\delta T \ll \tau\kappa T_M/Q$ calls for a possibly more severe criterion: $V \gg V_c\, mc_I/T_M\, QR/\gamma_0$, R denoting the mean interface curvature radius.

In practice, the latter criterion is usually an order of magnitude more restrictive than the former. In particular here, at a dendrite tip, $R = \rho \approx 10$ μm so that, with $\gamma_0/Q \approx 0.2$ nm, $QR/\gamma_0 \approx 5.10^4$. As, usually, mc_I is larger than 0.1 K and T_M of the order of 350 K, this criterion reads $V \gg 15V_c$ and even $V \gg 150V_c$ if mc_I is of the order of a Kelvin, as here. Usually, the temperature difference implied by thermal gradient thus stands in between those driven by solute concentration and surface tension: $\tau\kappa T_M/Q \ll \delta T \ll mc_I$. This means that, on a diffusion length, the interface is quasi-isotherm regarding solutal effects but largely nonisotherm regarding capillary corrections. The former property states that, at the diffusion-advection scale l_D, the interface can be considered as analogous to a freely growing interface part. However, the latter property warns us that surface tension effect and *a fortiori* those of anisotropy are likely to be overcompensated by the thermal gradient influence.

Skipping out this caveat has led a popular but insufficiently justified analogy between free growth and directional solidification at large velocity. According to it, considering the vicinity of the fastest growing point of a directional dendrite as a freely growing dendrite tip and leaving aside the competition between different sources of anisotropic corrections to its interface temperature, one might expect it to grow along a principal crystalline axis and involve a maximal curvature: $\mathbf{n}_c // \mathbf{V}_g // \mathbf{a}$.

2. Small Péclet number: $\mathrm{Pe} < 1$

At small Péclet number $\mathrm{Pe} < 1$, the influence length l_D of an interface point extends over the whole microstructure scale Λ. The interface dynamics is then nonlocal and involves interactions with neighbor microstructures. The smallest scale to consider is thus Λ and even more if the microstructures displayed on the interface look different. The temperature difference brought about on this scale by the thermal gradient is $\delta T = G\Lambda \approx mc_I \mathrm{Pe}_c$ where $\mathrm{Pe}_c = \Lambda V_c/D$ denotes the Péclet number at the planar interface destabilization. As usually Pe_c is at least 0.1 (as here), the interface cannot thus be considered as isothermal. Accordingly, the

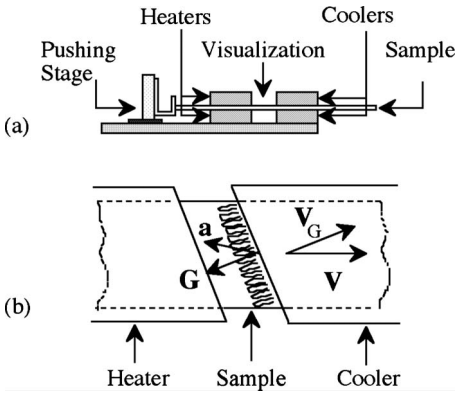

FIG. 1. Sketch of the experimental setup. (a) Side view. The sample is pushed at a prescribed velocity **V** in a controlled thermal gradient **G**. (b) Top view. The thermal gradient direction is monitored by turning the direction of the thermal boundaries. This enables its angle with a preferred crystalline direction **a** to be routinely changed. The projection of the pushing velocity **V** on the thermal gradient direction is labeled $\mathbf{V}_G$.

thermal gradient must play a dominant role on the cellular or dendritic form and thus, on both its growth direction and the location of its maximal curvature. In particular, the microstructure tip appears to be much more accurately described by a Saffman-Taylor finger [25–29] than by a free growth parabola. In addition, as its growth direction is close to that of the thermal gradient **G**, whatever the crystal orientation [20–22], its maximum curvature might be expected to point toward this common direction: $\mathbf{n}_c//\mathbf{V}_g//\mathbf{G}$. This is supported by the fact that the anisotropic corrections to the interface temperature T_I (1) are largely dominated by the temperature difference brought about by the thermal gradient on the tip.

3. Growth direction and maximal curvature

In directional solidification, both the maximum curvature and the growth direction are thus expected to turn from a crystallographic direction to the heat flow direction as the Péclet number decreases. This is well-known for the growth direction and has been largely documented in our experiment [20–22]. However, we shall show here that, contrary to this expectation, the maximal curvature keeps pointing toward the crystallographic direction for decreasing Pe, despite the increasing influence of the thermal gradient.

III. EXPERIMENT AND PROCEDURES

The experimental setup is designed so as to provide a nonintrusive observation of the directional solidification of a single microstructure layer. It thus consists in pushing, at a controlled velocity and in a prescribed thermal gradient, a thin sample of a transparent alloy. It is described in detail in references [4,22] and is briefly reported below (Fig. 1).

Heaters and coolers are made of copper blocks electronically regulated to better than 0.1 K. The sample is pushed in between them by a ball-screw driven stage coupled to a stepper motor by a 5 mm thread screw and a reductor of factor 74.1. The motor involves 6 400 microsteps per turn and is slowed at each step by Foucault current to prevent vibrations. This provides a regularity of the pushing velocity better than $\pm 3\%$, as controlled by a Michelson interferometer. The sample is long (15 cm), large (5 cm) and thin (50 μm). It is made by gluing together two glass plates separated by thin spacers. It is filled by capillarity with a transparent material, a succinonitrile ($C_4H_4N_2$) alloy purchased by Sigma Aldrich. Observations are made by visualizing on a CCD camera the distortions undergone by an initially parallel light beam crossing the sample. This enables the visualization of the interface as a sharp line of contrast.

Analysis of the alloy by nuclear magnetic resonance and by infrared spectroscopy identifies a single chemical bond other than those of succinonitrile: an ethylenic bond. This excludes contamination by common substances as water and points to ethylen or acrylonitrile as the dominant impurity.

The sample is thin enough to allow a single layer of cell or dendrite to grow in it. Compared to a 3D growth, this layer then experiences forced conditions imposed by the sample, i.e., thermal and solutal boundary conditions and a fixed thickness. The thermal conditions impose a thermal field which satisfies the temperature change imposed by heaters and coolers but in a sample that slowly drifts toward the latter. Temperature advection then weakly distorts the temperature field out of a linear variation (see appendix of [36]). However, the implication on the thermal gradient at the solidification interface is only of second order when the interface is placed, as here, in the middle of the gap [4]. Solutal boundary conditions impose a vanishing flux at the top and bottom boundaries. This, however, corresponds to the natural conditions encountered in 3D when the top and bottom neighbor layers are identical to the one they sandwich.

The effects of confinement in a direction normal to the sample can be addressed by phase field simulations. It then appears that, above a value of about $d=30$ μm, the influence of the sample thickness d on both the projected shapes and the undercooling of cells or dendrites is negligible [37]. This property echoes the independence of the critical velocity of planar destablization V_c on d in this domain [38]. It means that the two dimensions which define the cell boundaries, i.e., the sample thickness d and the cell spacing Λ, decouple so that the form and the dynamics of the two-dimensional (2D) interface seen from above actually refers to a 2D issue. This has been explicitly evidenced on the onset of sidebranching since its value for lateral (respectively, transversal) branching only depends on a single dimension, the dendrite spacing (respectively, the sample thickness), whatever the value of the remaining dimension [4].

Altogether, these properties show that the 2D interface visualized in thin samples here exhibit the same behavior as in 3D except that the third dimension, that of the sample thickness direction, is frozen. In particular, the independence of the microstructure undercooling on the sample depth d above $d=30$ μm points to a negligible influence of the out-of-plane curvature on the variations in interface temperature. We shall then overlook it in the following.

Succinonitrile is a body-centered crystal. To enable an accurate determination of its orientation and avoid grain

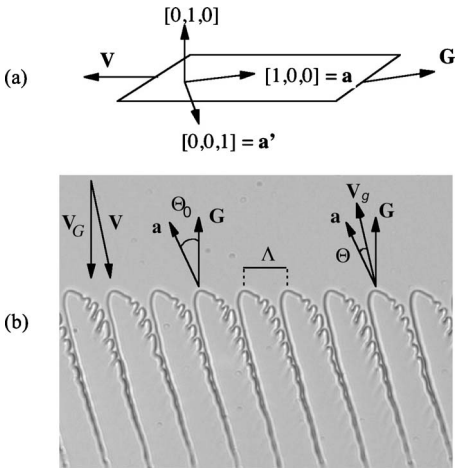

FIG. 2. Sketch of the relevant directions and variables: (a) directions of the principal crystalline axes with respect to the sample. One axis is normal to the plane. The remaining axis that is the closest to **G** is labeled **a**. This crystal defined direction corresponds to the growth direction of large velocity dendrites. (b) Thermal gradient **G**, crystal defined direction **a**, growth velocity $\mathbf{V}_g$, and microstructure spacing Λ. The angles $\Theta=(\mathbf{a},\mathbf{V}_g)$ and $\Theta_0=(\mathbf{a},\mathbf{G})$ measure the relevant directions with respect to **a**. The velocity of isothermal lines is given by the projection $\mathbf{V}_G$ of the pushing velocity **V** on the direction of **G**. Image width is 545 μm.

boundary competitions, a single crystal has been iteratively selected by a controlled solidification/fusion process. In particular, grain orientations have been evidenced from the growth directions of rapidly solidifying dendrites and have guided the selection of a single convenient grain.

Interestingly, one principal direction of the crystal proved to be normal to the sample to the accuracy of our observation [Fig. 2(a)]. This has been attested by the fourfold symmetry of the cross shape displayed by free dendrites and by the left/right symmetry of the sidebranches developed in the sample depth by directional dendrites. Although the observation of these symmetries do not exclude a slight tilt of crystal orientation off the sample normal, it restricts its angle to a few degrees at most. On the other hand, detailed studies of the effects of anisotropy in thin samples have shown that a relevant effective anisotropy to consider was that referring to an interface normal **n** belonging to the sample plane [39], i.e., to the 2D interface seen by projection along the sample normal. Then, by symmetry, anisotropy corrections should be even, and thus of second order, in the tilt angle. This property, together with the weakness of this angle, allows us to neglect this tilt here, if any, and thus to reduce crystal orientation to that of a vector in plane.

To identify this vector, it is convenient to consider a dendrite direction solely linked to the crystal orientation. This is provided by the growth directions of rapidly solidifying dendrites which actually prove to only depend on the crystal orientation, irrespective of the thermal gradient direction. Two of them, **a** and **a′**, one perpendicular to the other, are displayed in the sample plane [Fig. 2(a)]. We shall call hereafter **a** that corresponding to the asymptotic growth direction of the dendrites under study. In practice, it corresponds to the closest direction to **G**.

To finely control the misorientation angle $\Theta_0=(\mathbf{a},\mathbf{G})$ between the thermal gradient **G** and the crystal defined direction **a**, we preferred varying the former which is macroscopically established rather than the latter which is microscopically controlled by growing germs. This has been achieved by designing the boundaries of heaters and coolers so as to rotate the thermal gradient by prescribed angles [Fig. 1(b)]. Several rotation angles of **G** were used on several crystal orientations so as to span the range $[0°,45°]$ for Θ_0.

Measurements of dendrite growth directions were achieved from the recordings of their tip trajectories as they drift in the observation field [22]. This field corresponds to the rectangular video frame, $(X,Y)=(768,512)$ pixels wide, oriented so that its Y axis is parallel to the pushing velocity **V**. The tilt angle $\alpha=(\mathbf{V}_g,\mathbf{V})$ of dendrite growth directions with respect to the pushing velocity **V** then writes $\tan(\alpha)=X/y$ where y denotes the distance made on the Y axis by a dendrite tip during its drift in the video frame. As this distance is computed from the drift time T by a linear relationship, $y=VT$, its relative uncertainty writes $\delta y/y=\delta T/T$. Here, the uncertainty on T follows from the uncertainty in localizing the dendrite tip on the interface or, equivalently, in determining the interface length L in the video frame from the drift of a dendrite along it. This means that, denoting V_d the dendrite drift velocity on the interface, T follows from L by a linear relationship too, $T=L/V_d$, so that its relative uncertainty reads $\delta T/T=\delta L/L$. With $\alpha<45°$, $\delta L=1$, $L>X$ and $X=768$ in pixel units, this finally yields $\delta\alpha=\sin(2\alpha)\delta y/2y<1/2X<0.04°$. The same uncertainty is found for the angles $(\mathbf{V},\mathbf{G})$ and $(\mathbf{V},\mathbf{a})$, thereby yielding, for the angles $\Theta_0=(\mathbf{a},\mathbf{G})$ and $\Theta=(\mathbf{a},\mathbf{V}_g)$ [Fig. 2(b)], a net uncertainty less than 0.1°.

The succinonitrile alloy displayed a melting point of 56 °C, close to the melting point of the pure substance, 58.1 °C. The solutal diffusivity has been measured at $D=1350\pm50$ μm^2.s^{-1} and the partition coefficient of the melt at $k=0.29\pm0.05$. The thermal gradient was fixed at $G=70$ K·cm^{-1}. It provided a critical velocity of about $V_c=1.15$ μm.s^{-1}. Pushing velocities and microstructure spacings varied from $V=5$ to 50 μm.s^{-1} and from $\Lambda=70$ to 230 μm.

IV. MICROSTRUCTURE EVOLUTIONS

Figure 3 reports a series of snapshots showing the evolution of microstructures with velocity V and misorientation angle Θ_0. In each of them, to a good accuracy, the line joining the microstructure tips corresponds to an isothermal line [40] and the microstructure axes are close (but not equal) to the microstructure growth directions [22]. The angle between these two lines then provides with the naked eye the departure of growth directions from the thermal gradient direction **G**. Dendrite tilting is thus found to increase with either the velocity or the misorientation angle Θ_0.

At large Θ_0 and small V, one notices a transition to a repetitive tip-splitting mode, so-called degenerate mode, which prevents a definite growth direction to be identified [Figs. 3(p) and 3(q)]. Other instabilities, not displayed here, bound the allowable spacing by nucleation or elimination of

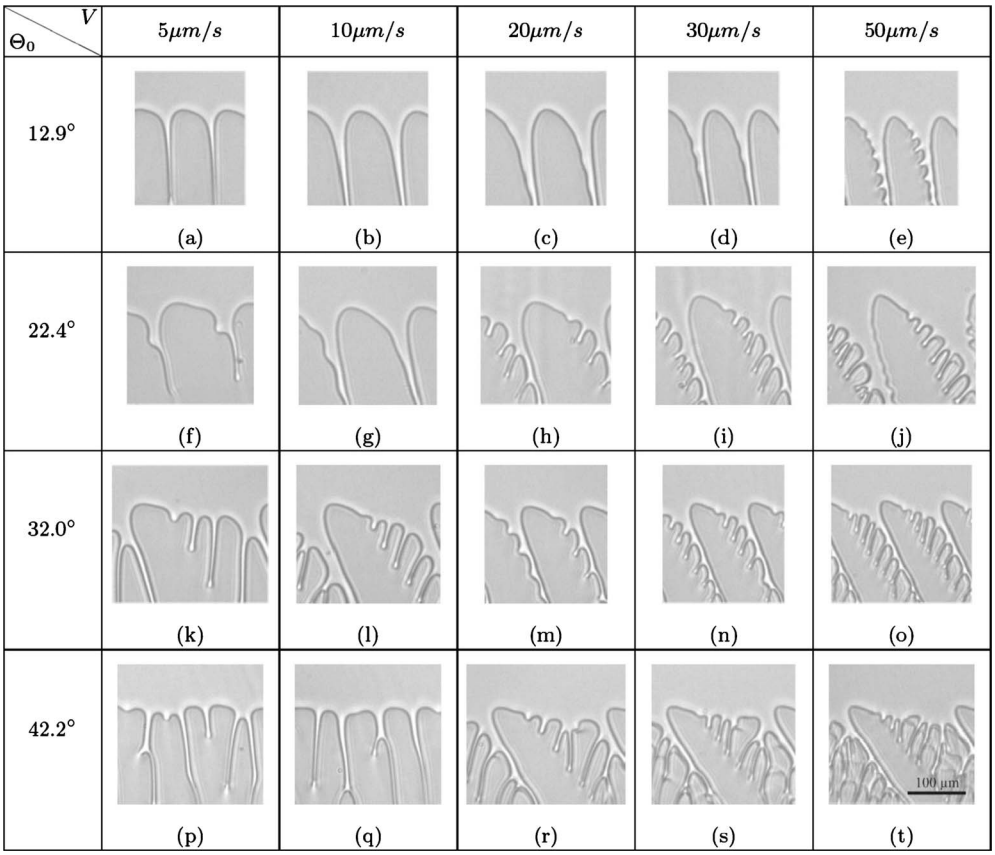

FIG. 3. Experimental library showing the forms of microstructures and their tilt from the thermal gradient direction **G** to the crystal defined direction **a**. The direction of **G** is normal to the line joining the microstructure tips. The direction **a** is close to the microstructure axes at large velocity. Their angle is labeled $\Theta_0=(\mathbf{a},\mathbf{G})$. The structures in (p) and (q) stand in the so-called degenerate mode where iterative tip splittings prevent a permanent direction to be defined. In the remaining pictures, tilting, asymmetry and sidebranch development increase with velocity V or misorientation angle Θ_0. The scale is the same for all figures and is given in figure (t) by a 100 μm line.

a microstructure [41–43]. Within the allowable band, various stable spacings can then be obtained on homogeneous patterns depending on the growth history [4,43].

As dendrite tilting increases, the asymmetry of cells and dendrites gets more pronounced. In particular, in the vicinity of their tip, the interface standing on the side of the tilting gets more rounded than on the opposite side. In addition, its groove remains smooth whereas that on the opposite side develops sidebranches. Finally, the distance between dendrites raises with tilting, as a result of sidebranches succeeding in reaching the isothermal line joining the dendrite tips.

These observations reveal a large implication of crystal orientation on the growth directions and the morphologies of microstructures. In particular, even at large velocities where dendrite growth directions are ascribed to the direction **a**, important variations in morphologies are in order depending on whether the misorientation angle Θ_0 is small [Fig. 3(e)] or large [Fig. 3(t)]. In the first case, nearly symmetric dendrites are displayed whereas, in the latter case, largely asymmetric dendrites exhibiting a long sidebranch wake and a wide spacing are in order.

V. GEOMETRICAL MEASURE OF LOCAL CURVATURE

We aim at measuring local curvatures along solidification interfaces in the vicinity of the microstructure tips. For convenience, we begin by rotating the interface images of the angle Θ_0, so that from now on the vertical axis will be aligned with the crystal defined direction **a** on all images. It appears that this makes the microstructure tips nearly symmetric with respect to the direction **a**. As a result, microstructures will thus be treated almost similarly by the forthcoming algorithms.

We select the most curved steady part of the tip i.e., for dendrites, the tip region which experiences no branching and, for cells, their ahead region which is indeed the most curved part of them (Fig. 3). We then obtain a numerical profile of the interface by the following process.

We first extract a skeleton along which a more detailed localization of the interface is sought. This is achieved by use of the intensity modulation profile found on the interface normal. As reported in figure Fig. 4(a), this profile is made of a sharp raise followed by a small decrease toward a plateau. We used it to unambiguously locate the interface as the location of the sharp maximum. For this, at each point of the skeleton, we considered a box, 48 pixels long, 8 pixels large, in which a linear combination of an inverse hyperbolic tangent function and a Gaussian function is fitted onto the normal profile. This provided us with both the interface locations and their uncertainties.

Following the irregularities of the skeleton [Fig. 4(b)], the interface curve shows slight steady modulations at the micro-

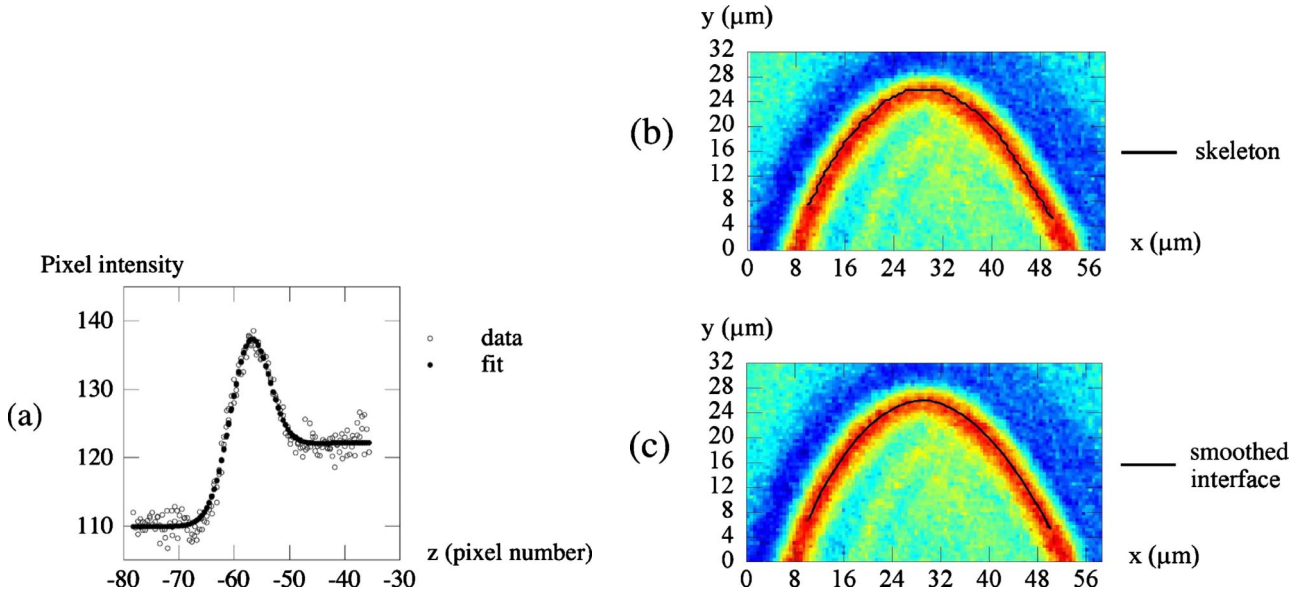

FIG. 4. (Color online) Digitalization processing. A rotation of angle Θ_0 of the coordinates has been applied to the experimental images, so that the **y** axis is aligned onto the crystal defined direction **a**. Here $\Theta_0=12.9°$ and $V=30\ \mu m.s^{-1}$. (a) Intensity profile along the normal to an interface skeleton. The interface location is taken at the intensity peak. (b) Interface skeleton obtained after thresholding. Colors (gray levels) indicate the pixel intensity. The skeleton lies in the red (dark gray) zone of large pixel intensity (larger than 130). Pixel intensity then decreases to about 125 in the light blue (light gray) dendrite interior and to about 110 in the dark blue (dark gray) zone which surrounds the dendrite. (c) Smoothed interface obtained by improving its localization using the intensity profile (a) and by smoothing out spurious fluctuations at the micrometric scale.

metric scale of a pixel. Usually, they would have been weak enough to be overlooked. However, here, the determination of local curvatures requires a fine spatial analysis of the interface which would suffer from these perturbations. In particular, a weak distortion of the interface profile, even localized, would be sufficient to induce a large change of the interface normals and thus, of the interface curvature. However, no such steady distortion can be physically generated on the interface at such a small scale, in particular following the smoothing effects of capillarity. It is therefore legitimate to eliminate them before proceeding further. For this, we apply a gliding parabolic fit performed on window widths of the order of the third of the mean curvature radius. As this smoothing process is convergent, we apply here iteratively to obtain the interface curve at the required smoothness for curvature determination. As shown on Figs. 4(b) and 4(c), the resulting curve is hardly distinguishable from the initial skeleton with the naked eye. However, it ensures a signal to noise ratio weak enough for applying the fine differential analysis of the interface profile that is next required (Fig. 5). In addition, as the fluctuation scales filtered out are much smaller than both the local curvature radii of the interface and their spatial scale of variation, no significant drift of the value of these radii or of the localization of their minimum can be induced by the filtering. This has been checked by applying additional random small scale perturbations to the initial skeleton, as reported in the next section.

We now turn to the determination of local curvatures on the interface tip. Usually, the curvature of a curve at a point is determined as the curvature of tangent circles or best fitting parabolas at that point [6,44]. These procedures however raise intrinsic difficulties which originate from the fact that the interface is neither a circle nor a parabola [14,45], especially in directional solidification [29]. Then, determining a tangent circle to a curve requires either a large data density in the vicinity of the contact point or, on the negative, a fit on some extended area around it. In the second case, actually the most usual, the resulting curvature radius is not local but refers to a mean curvature over some interface area. Fitting to parabolae raises similar concerns which may yield to consider quadratic corrections to the interface shape [45,46]. In particular, the best fitting parabola evolves with the extent of the interface part that is considered so that enlarging it makes curvature radius first increase, then stagnate and finally de-

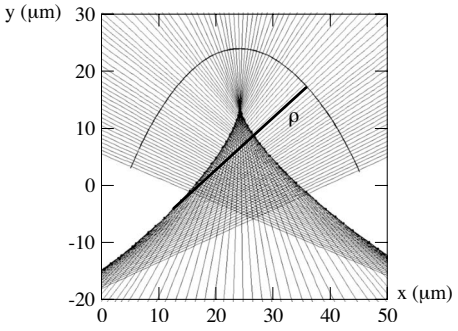

FIG. 5. Determination of local curvature radii by intersection of curve normals. The intersection of two neighbor normals provides the center of the circle tangent to this interface part. This geometrical property yields an accurate measurement of local curvature radii ρ. The envelop of the normals displays a cusp singularity whose turning point refers to a minimal curvature radius. Here $\Theta_0=12.9°$, $V=30\ \mu m.s^{-1}$ and the interface is that displayed on Fig. 7(d) and in Fig. 4.

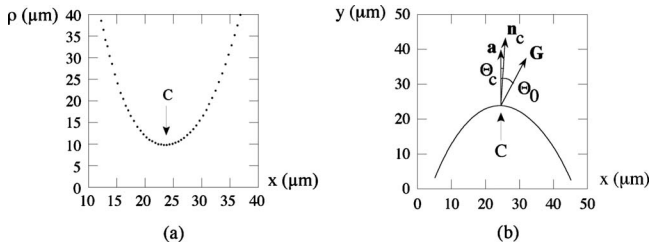

FIG. 6. Analysis of curvature radii and normal orientations on a solidification interface. Here $\Theta_0=12.9°$ and $V=30\ \mu\mathrm{m.s}^{-1}$ and the interface is that considered in Figs. 4 and 5. The distance x refers not to the curvilinear abscissa but to a Cartesian abscissa on the axis normal to direction **a**. (a) Evolution of the curvature radius with the abscissa of interface points. A minimal curvature radius is reached at a point C. (b) Relevant directions at point C: the interface normal $\mathbf{n}_c$, the crystal defined direction **a** and the thermal gradient **G**.

crease again [28]. A local measure of curvature radius would thus require to restrict analysis to a small interface part but at the prejudice of the fit accuracy.

In view of this, we preferred returning to the definition of curvature radius ρ as the rotation rate of tangent vectors τ on a curve: $d\tau/ds=-\mathbf{n}/\rho$ where s denotes the curvilinear abscissa and **n** the curve normal. Writing, in complex coordinates, $\tau=\exp(i\theta)$ and $\mathbf{n}=-i\exp(i\theta)$ yields $d\theta/ds=1/\rho$ where θ denotes the angle between a fixed direction $\mathbf{e}_x$ and the tangent vector τ. This in particular means that, for an arbitrary elementary displacement δs on the curve, the resulting normals would intersect at a distance $\rho(s)$ (Fig. 5). This geometrical property offers the opportunity of performing a local measure of curvature radius by a simple but accurate mean.

The advantage of this measurement procedure is to be accurate even on small portions of the interface and to be independent of the global size of the form to analyze. In particular, here, the measure $\rho(s)$ is not sensitive to the displacement δs that is considered, provided that δs remains much weaker than $\rho(s)$ and that fluctuations at the scale δs are absent or smoothed out, as done here. Another advantage of this procedure is to provide a global geometrical view of the evolution of local curvatures from the figure made by the set of intersecting normals: the curve evolute (Fig. 5). In particular, the normals envelop displays a cusp singularity similar to a caustic in optics and whose turning point refers to the minimal curvature radius on the interface.

VI. NORMAL DIRECTION AT THE MAXIMAL CURVATURE AND CRYSTAL ORIENTATION

The typical evolution of curvature radii along a solidification interface is reported in Fig. 6(a). They are found to start from large values in a groove, then decrease to a minimum on the microstructure tip and finally increase again on the opposite groove.

We call C the point where the curvature radius is minimal. Our issue consists in investigating a possible link between this point and the crystal orientation. For this, we report on Fig. 6(b) the crystal defined direction **a** and the normal direction $\mathbf{n}_c$ to the interface at point C with, for completion, the thermal gradient direction **G**.

Interestingly, it appears that the interface normal $\mathbf{n}_c$ at point C stands very close to the crystal defined direction **a**. Looking to Fig. 7 reveals with the naked eye that this property seems to qualitatively extend to the whole microstructure library, whatever the Péclet number or the misorientation angle Θ_0. In particular, as in Fig. 6(b), the largest curvatures seem to be located at the top of the interfaces, i.e., at locations where the interface normal is parallel to direction **a**.

To quantitatively analyze the closeness between directions $\mathbf{n}_c$ and **a**, we introduce the angle $\Theta_c=(\mathbf{a},\mathbf{n}_c)$ and compare it to the misorientation angle $\Theta_0=(\mathbf{a},\mathbf{G})$ which sets the variation range of the growth direction angles Θ. For this, we plot

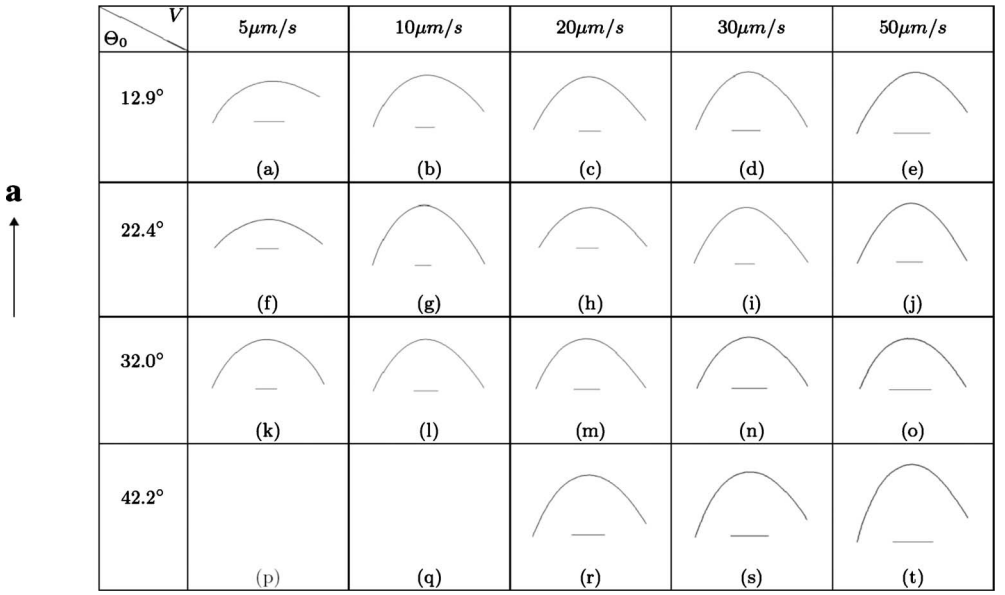

FIG. 7. Digital smoothed forms of the solidification interfaces listed in Fig. 3 (except those displaying a degenerate mode [Figs. 3(p) and 3(q)]). The bottom-up axis points toward the crystal defined direction **a**. On each form, a thin line indicates a scale of 100 μm.

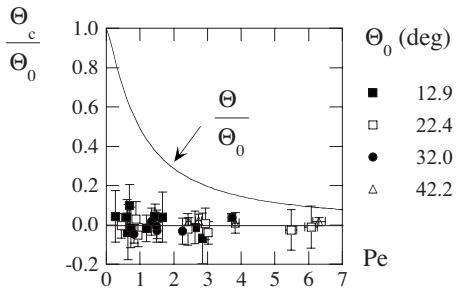

FIG. 8. Comparison between growth directions $\mathbf{V}_g$ and the normal $\mathbf{n}_c$ at the most curved point C at various Péclet numbers Pe. Data points correspond to the reduced angles Θ_c/Θ_0 with $\Theta_c=(\mathbf{a},\mathbf{n}_c)$. The curve refers to the reduced angles Θ/Θ_0 with $\Theta=(\mathbf{a},\mathbf{V}_g)$. Whereas growth directions rotate from $\mathbf{G}$ to $\mathbf{a}$ (i.e., Θ from Θ_0 to 0), the most curved point C keeps pointing toward direction $\mathbf{a}$ (i.e., $\Theta_c=0$), whatever the Péclet number.

in Fig. 8 with respect to the Péclet number Pe the reduced angles Θ_c/Θ_0 and the curve Θ/Θ_0(Pe) determined from previous studies in the same system [20–22]. In agreement with their expected behaviors, both reduced angles are close to zero at large Pe. However, at low Pe, whereas the reduced growth direction Θ/Θ_0 largely departs from zero to reach unity at vanishing Pe, the reduced angle Θ_c/Θ_0 remains close to zero on the whole Péclet range, even at the lowest Péclet studied. This corroborates the qualitative impression that interface normals $\mathbf{n}_c$ remain comparatively much closer to the crystal defined direction $\mathbf{a}$ than to the thermal gradient direction $\mathbf{G}$ on the whole microstructure library (Fig. 7). The difference with the behavior of the growth direction $\mathbf{n}_g=\mathbf{V}_g/V_g$ is exemplified in Fig. 9 on two interfaces referring to low or large Péclet number.

On the graph of Fig. 8, the error bars on Pe result from the uncertainties on Λ and V and those on the reduced angles Θ_c/Θ_0 from the uncertainty on the interface forms. The latter uncertainty mainly originates from thresholding, following the fluctuations of intensity of the dark and bright zones that

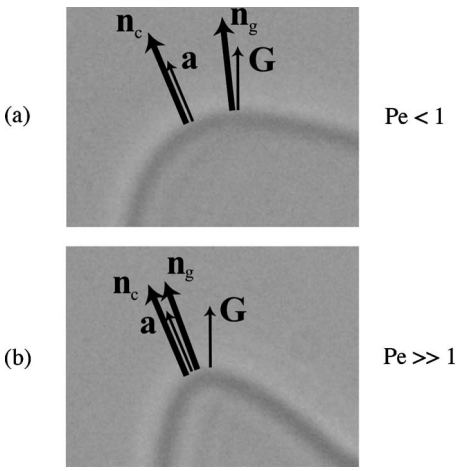

FIG. 9. Characteristic directions on interface tips at low (a) or large (b) Péclet numbers. Here, $\mathbf{n}_c$ refers to the interface normals at the most curved point C and $\mathbf{n}_g=\mathbf{V}_g/V_g$ to the growth direction. The shapes in (a) and (b) correspond to those, respectively, labeled (f) and (j) in Figs. 3 and 7.

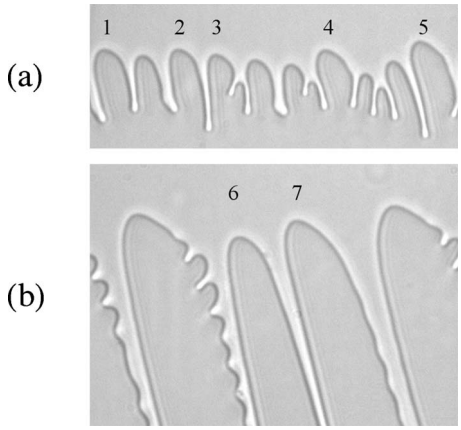

FIG. 10. Unsteadiness and spacing gradients. Transients induced by planar destabilization (a) or dendrite elimination (b). Here $\Theta_0=22.4°$ and the figure widths are 495 μm. The numbered microstructures are analyzed in Table I. (a) Sudden step from $V=0$ to 20 $\mu\mathrm{m.s}^{-1}$. (b) $V=20$ $\mu\mathrm{m.s}^{-1}$.

surround the interface, and to a lesser extent from data processing. In view of the number of processing stages, some of them nonlocal, and of the difficulty of accurately determining their intrinsic uncertainties, we have preferred evaluating their net resulting uncertainty by the following pragmatic approach. We first apply random perturbations to the digitalized interfaces with an amplitude equal to that observed on the images, as quantified by the fit of the normal intensity profile [Fig. 4(a)]. We then apply the remaining processing and determine the resulting variations $(\delta\rho(s),\delta\Theta_c)$ in the curvature radii $\rho(s)$ and the angles Θ_c. The absolute variations $\delta\Theta_c$ obtained this way provide a direct estimate of the uncertainty of the angle measurements. They amount to $\pm 2°$ whatever the Péclet number. The corresponding relative uncertainties $\delta\Theta_c/\Theta_0$ are indicated by error bars on Fig. 8.

The microstructures reported in the library of Fig. 3 were in a homogeneous and permanent state in the sense that microstructures displayed the same form and the same spacing on the interface and that, apart from branching, no evolution of form or of spacing was in order. To investigate whether the link between maximal curvature and crystal orientation extends beyond these particular states, we have addressed time-dependent microstructures and spatially inhomogeneous interfaces. Time-dependence was considered through the development of the Mullins-Sekerka instability on a planar front suddenly pushed at a velocity of 20 $\mu\mathrm{m.s}^{-1}$, i.e., about $17V_c$ [Fig. 10(a)] and through the microstructure dynamics induced by a dendrite elimination at $V=20$ $\mu\mathrm{m.s}^{-1}$ [Fig. 10(b)]. Seven microstructures were analyzed. To our uncertainty, they displayed in Table I vanishing angles Θ_c and vanishing reduced angles Θ_c/Θ_0, the amplitude of the latters being below 0.1 for all. The coincidence between an interface normal aligned with the direction $\mathbf{a}$ and a maximal local curvature thus extends to these transient states.

VII. DISCUSSION

To better discuss our results, let us summarize them by introducing, in complement to the most curved point C, the

TABLE I. Angle $\Theta_c=(\mathbf{a},\mathbf{n}_c)$ between the normal direction $\mathbf{n}_c$ at the most curved point C and the crystal defined direction $\mathbf{a}$ on the time-dependent microstructures of Fig. 10. This angle fluctuates around 0° and remains far from the misorientation angle $\Theta_0=22.4°$ as shown by the low relative values of Θ_c/Θ_0.

Dendrite's number	Θ_c (deg)	$\Theta_0-\Theta_c$ (deg)	Θ_c/Θ_0
1	−0.13	22.53	−0.006
2	0.05	22.35	0.002
3	1.14	21.26	0.051
4	0.34	22.06	0.015
5	1.59	20.81	0.071
6	−1.01	23.41	−0.045
7	1.65	20.75	0.074

following interface points: the quickest growing point Q, the hottest point H and the point A growing toward direction $\mathbf{a}$. Here the interface dynamics is considered within the normal gauge according to which the interface points move normally to the interface. Then points A, Q, H satisfy $\mathbf{n}_A//\mathbf{a}$, $\mathbf{n}_Q//\mathbf{V}_g$ and $\mathbf{n}_H//\mathbf{G}$. In particular, as microstructures globally move at growth velocity $\mathbf{V}_g$, normal velocities $\mathbf{V}_n=V_n\mathbf{n}$ satisfy $V_n=\mathbf{V}_n\cdot\mathbf{n}=\mathbf{V}_g\cdot\mathbf{n}\leq V_g$, thereby yielding the criterion for the quickest point Q.

The four points C, A, Q, H, are sketched on Figs. 11(a) and 11(b) together with their evolution in our experiment. Our main evidence is that the most curved point C remains close to point A whatever the Péclet number and the thermal gradient $\mathbf{G}$, i.e., whatever the spacing Λ, the diffusion length $l_D=D/V$ and the direction of $\mathbf{G}$ [Figs. 11(a) and 11(b)].

In comparison, in free growth, apart from the atypical directions sometimes displayed [16], $Q=A$ since dendrites grow toward a principal crystalline direction, and $C=A$ since they are then symmetric. Point A then corresponds to a minimum of both stiffness and curvature, and thus of the interfacial undercooling. Labeling the interface point of minimal undercooling Δ, one thus obtains $A=C=Q=\Delta$. Accordingly,

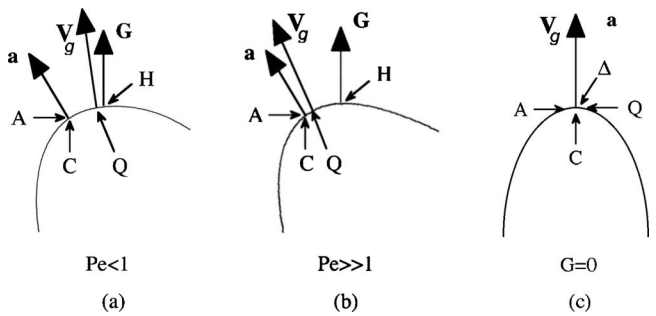

FIG. 11. Sketch of relevant directions and characteristic points in directional (a,b) and free (c) solidification. Points respectively refer to a normal pointing toward the crystal defined direction $\mathbf{a}$ (A), to the most curved point C, the quickest point Q, the hottest point H and an extremal undercooling (Δ). (a) and (b) Directional solidification. Point C remains stuck to point A but point Q goes from H to A as Pe increases. (c) Free solidification. The four points A,C,Q,Δ remain confused one with the other at any velocity.

in free growth, the relative evolution of these points raises no question since they are all confused. In contrast, in the present directional solidification, the difference between A and H allows Q to go from A to G as Pe decreases while C surprisingly remains located at A, whatever the growth regime and the growth parameters.

The persistence of point C on point A whatever the diffusion length and the thermal gradient orientation is quite intriguing. It actually states the insensitivity of the location of the maximal curvature to the growth direction $\mathbf{V}_g$ and to the thermal gradient $\mathbf{G}$, even at low growth velocity where the interface points are the most coupled by diffusion, the growth directions the most distant from the crystal defined direction $\mathbf{a}$ and the microstructure shapes the most modified by the thermal gradient. This seems to indicate that C surprisingly only refers to local considerations, independently of the distance to neighbor dendrites, of diffusion effects or of isothermal lines.

Whereas the local dependence of C remains to be legitimized, we notice that it is self-consistent owing to the following considerations. Consider an elementary circular part of a curved interface involving a surface tension γ_0 and introduce interfacial anisotropy while assuming a local dynamics. According to (1) (2), the increase δT_I of the interface equilibrium temperature T_I brought about by anisotropy will be the largest for an interface normal $\mathbf{n}$ pointing toward direction $\mathbf{a}$: $\delta T_I=15\epsilon_4\cos(4\theta)\gamma_0\kappa T_M/Q$ here with $\theta=(\mathbf{a},\mathbf{n})$. It will thus induce an interface bulge there, yielding an increase of curvature κ and, finally, a further amplification of the anisotropy effects. This feed-back loop thus goes toward the formation of small curvature radius at the point where the interface normal points toward direction $\mathbf{a}$. That neither the thermal gradient nor the diffusion field from other interface parts parametrize the location of the most curved point C remains however to explain. Similarly, the fact that the most curved part of the interface is solely set by a nanometric phenomenon, the crystalline anisotropy, independently of the sub-millimetric phenomena linked to diffusion, advection or heat flow remains to elucidate.

In contrast with the most curved point C, the quickest point Q moves with Pe from the hottest point H to point A [Figs. 11(a) and 11(b)]. This means that the most curved point is thus no longer the quickest one, as it is in free growth. This statement apparently goes against the tip power principle following which curvature enhances diffusion and thus growth velocities. This is because of the presence of the thermal gradient which also parametrizes the interface position and thus its normal velocity.

Whereas the property $C=A$ remains to be explained, it provides a useful geometrical implication of crystalline anisotropy at the scale of the microstructure: the part of the interface pointing toward the crystal defined direction $\mathbf{a}$ is the most curved. If confirmed in 3D, this would enable the crystalline direction to be identified from the sole analysis of the interface. In thin samples and on the present 2D interfaces, this property might be a valuable mesoscopic information for further understanding the position of the quickest point Q and thus the direction of the growth velocity $\mathbf{V}_g$. Similarly, it might be a relevant information for understanding the overall shape of microstructures and thus their resulting segregation.

VIII. CONCLUSION

Crystal anisotropy is known to play an important role in the stability of directionally solidified microstructures and in the tilting of their growth directions away from the thermal gradient direction. In particular, dendrites grow at large Péclet number Pe in a direction **a** solely set by the crystal orientation and, at low Pe, in a direction solely set by the thermal gradient **G**. The mechanism by which the tiny modulations of temperature interface implied by crystal anisotropy succeed in orientating the whole microstructure remains an important issue to clarify for fundamental understanding and metallurgical applications.

Here, we have evidenced experimentally another, more geometrical, implication of crystal anisotropy: the largest interface curvature is located at a point whose normal growth is aligned with the crystal defined direction **a**. This property has been found to be valid on all cells or dendrites, whatever the Péclet number, the thermal gradient direction, the crystal orientation, the steadiness or the spatial homogeneity of the microstructure pattern. Whereas it is known to largely apply in free growth, its extension to directional solidification remains puzzling. In particular, the additional presence of the thermal gradient might have been thought capable of significantly shifting the location of the most curved point. This possibility is stressed by the actual tilting of growth directions away from the direction **a** imposed by the thermal gradient. The reason for which the thermal gradient succeeds in monitoring growth directions but not the location of the largest interface curvature remains to be elucidated. Conversely, the geometrical link between crystal direction and interface curvature might be used to shortcut the microscopic influence of the crystal lattice on the overall microstructure so as to reach a better understanding of the mechanisms governing dendrite morphology, dendrite tilting and therefore, dendrite microsegregation.

[1] B. Chalmers, *Principles of Solidification* (Wiley, New York, 1964); M. C. Flemings, *Solidification Processing* (McGraw-Hill, New York, 1974); W. Kurz and D. J. Fischer, *Fundamentals of Solidification* (Trans tech Publications, Zurich (1984).

[2] C. Jaupart and S. Tait, J. Geophys. Res. **100**, 17615 (1995).

[3] W. W. Mullins and R. F. Sekerka, J. Appl. Phys. **35**, 444 (1964).

[4] M. Georgelin and A. Pocheau, Phys. Rev. E **57**, 3189 (1998).

[5] J. S. Langer and H. Müller-Krumbhaar, Acta Metall. **26**, 1681 (1978).

[6] S. C. Huang and M. E. Glicksman, Acta Metall. **29**, 701 (1981); **29**, 717 (1981).

[7] R. C. Brower, D. A. Kessler, J. Koplik, and H. Levine, Phys. Rev. A **29**, 1335 (1984); D. A. Kessler, J. Koplik, and H. Levine, Adv. Phys. **37**, 255 (1988).

[8] J. H. Bilgram, M. Firmann, and E. Hurlimann, J. Cryst. Growth **96**, 175 (1989).

[9] J. S. Langer, Phys. Rev. A **33**, 435 (1986).

[10] E. Brener , H. Müller-Krumbhaar, and D. Temkin, EPL **17**, 535 (1992).

[11] T. Ihle and H. Müller-Krumbhaar, Phys. Rev. E **49**, 2972 (1994).

[12] S. Akamatsu and G. Faivre, Phys. Rev. E **58**, 3302 (1998); B. Utter and E. Bodenschatz, *ibid.* **66**, 051604 (2002).

[13] A. Papapetrou, Z. Kristallogr. **92**, 89 (1935); G. P. Ivantsov, Dokl. Akad. Nauk SSSR **58**, 567 (1947).

[14] E. Brener and D. Temkin, Phys. Rev. E **51**, 351 (1995).

[15] U. Bisang and J. H. Bilgram, Phys. Rev. E **54**, 5309 (1996).

[16] T. Haxhimali, A. Karma, F. Gonzales, and M. Rappaz, Nat. Mater. **5**, 660 (2006).

[17] R. Trivedi, Appl. Mech. Rev. **43**, S79 (1990); R. Trivedi, V. Seetharaman, and M. A. Eshelman, Metall. Trans. A **22**, 585 (1991).

[18] T. Okada and Y. Saito, Phys. Rev. E **54**, 650 (1996).

[19] S. Akamatsu and T. Ihle, Phys. Rev. E **56**, 4479 (1997).

[20] J. Deschamps, M. Georgelin, and A. Pocheau, EPL **76**, 291 (2006).

[21] A. Pocheau, J. Deschamps, and M. Georgelin, JOM **59**, 71 (2007).

[22] J. Deschamps, M. Georgelin, and A. Pocheau, Phys. Rev. E **78**, 011605 (2008).

[23] G. L. Ding and S. N. Tewari, J. Cryst. Growth **236**, 420 (2002).

[24] B. J. Spencer and H. E. Huppert, Acta Mater. **45**, 1535 (1997).

[25] P. Pelcé and A. Pumir, J. Cryst. Growth **73**, 337 (1985).

[26] P. Kurowski, C. Guthmann, and S. de Cheveigné, Phys. Rev. A **42**, 7368 (1990).

[27] M. Mashaal, M. Ben Amar, and V. Hakim, Phys. Rev. A **41**, 4421 (1990).

[28] M. Georgelin and A. Pocheau, J. Cryst. Growth **268**, 272 (2004).

[29] A. Pocheau and M. Georgelin, Phys. Rev. E **73**, 011604 (2006).

[30] E. A. Brener and V. I. Mel'nikov, Adv. Phys. **40**, 53 (1991); E. A. Brener and H. Levine, Phys. Rev. A **43**, 883 (1991).

[31] S.-K. Chan, H.-H. Reimer, and M. Kahlweit, J. Cryst. Growth **32**, 303 (1976).

[32] R. J. Schaefer, M. E. Glicksman, and J. D. Ayers, Philos. Mag. **32**, 725 (1975).

[33] M. Muschol, D. Liu, and H. Z. Cummins, Phys. Rev. A **46**, 1038 (1992).

[34] M. E. Glicksman, R. J. Schaefer, and J. D. Ayers, Metall. Trans. **7**, 1747 (1976).

[35] C. A. Wulff and E. F. Westrom, J. Phys. Chem. **67**, 2376 (1963).

[36] A. Pocheau, S. Bodea, and M. Georgelin, Phys. Rev. E **80**, 031601 (2009); M. Georgelin, S. Bodea, and A. Pocheau, EPL **77**, 46001 (2007).

[37] S. Gurevich, A. Karma, M. Plapp, and R. Trivedi, Phys. Rev. E **81**, 011603 (2010).

[38] S. de Cheveigné, C. Guthmann, and M. M. Lebrun, J. Phys. **47**, 2095 (1986).

[39] S. Akamatsu, G. Faivre, and T. Ihle, Phys. Rev. E **51**, 4751 (1995).

[40] A. Pocheau and M. Georgelin, J. Cryst. Growth **206**, 215 (1999).
[41] W. D. Huang, X.G. Geng, and Y. H. Zhou, J. Cryst. Growth **134**, 105 (1993).
[42] M. Georgelin and A. Pocheau, Phys. Rev. Lett. **79**, 2698 (1997).
[43] A. Pocheau and M. Georgelin, J. Cryst. Growth **250**, 100 (2003).
[44] A. Dougherty, J. Cryst. Growth **110**, 501 (1991).
[45] J. C. LaCombe, M. B. Koss, V. E. Fradkov, and M. E. Glicksman, Phys. Rev. E **52**, 2778 (1995).
[46] J. Maurer, B. Perrin, and P. Tabeling, EPL **14**, 575 (1991).